Arabian Journal of Geosciences (2019) 12: 226
https://doi.org/10.1007/s12517-019-4370-8

ORIGINAL PAPER

Country-scale discontinuity analysis of AW3D30 and SRTM Global DEMS: case study in Turkey

Umut G. Sefercik[1] · Umit Gokmen[2]

Received: 8 January 2019 / Accepted: 22 February 2019 / Published online: 19 March 2019

Abstract

The quantitative model of the Earth is provided by optical and radar space-borne remote sensing global digital elevation models (GDEMs). GDEMs are fundamental for many geo-spatial analysis and demanded by several applications that need topographical data. Recently released ALOS World 3D 30 m (AW3D30) and 1 arc-second (~30 m) Shuttle Radar Topography Mission (SRTM) C-band GDEMs have the advantages of high quality and free availability from JAXA and NASA and much in demand in scientific community. In this paper, we comprehensively analyzed the discontinuities between AW3D30 and SRTM C-band GDEMs in country-scale calculating and interpreting the influence of terrain inclination and land cover classes. The coherence between two GDEMs was estimated by absolute horizontal and vertical accuracy analysis in the basis of model-to-model validation approaches. During the analysis, standard deviation and normalized median absolute deviation of height differences between GDEMs were utilized as the main coherence indicators. The frequency distribution of height differences and the incoherent outliers were presented by error distribution graphics and height error maps, respectively. The results clearly demonstrated the significance of ascending and descending orbits, terrain inclination, and land cover on the discontinuities.

Keywords AW3D30 · SRTM · GDEM · Discontinuity · Coherence · Height error map

Introduction

Three-dimensional (3D) digital cartographic representation of the Earth surface is depicted by Digital Elevation Models (DEM). DEM is an indispensable product for large variety of disciplines such as mapping, 3D city planning, forestry, disaster monitoring and management, and agriculture, as well as Earth sciences. Formerly, DEMs were generated for local up to regional scale due to the limitations of ground surveying and photogrammetry. The main reasons of the limitations are high cost and time consuming processing in wider than regional areas. With the improvements in space-borne remote sensing technologies, DEM acquisition is possible not only in regional scale but also in global scale. Global DEMs (GDEMs) make possible to work on countries and continents and used in wide range of applications (Gianinetto 2009; Martino et al. 2009; Carvalho et al. 2010; Bullard et al. 2011; DeLong et al. 2012; Heckmann et al. 2012; Schneider et al. 2012; Sefercik et al. 2018). Space-borne GDEMs are derived by two main techniques as optical stereoscopy (Li et al. 2002; Toutin 2002; Lee et al. 2003; Kaczynski et al. 2004; Bahuguna and Kulkarni 2005; Cuartero et al. 2005; Toutin 2008; Radhadevi et al. 2010; Hobi and Ginzler 2012) and interferometric synthetic aperture radar (InSAR) (Soergel et al. 2003, 2009; Sefercik and Soergel 2010). In this paper, Advanced Land Observing Satellite (ALOS) World 3D 30 m (AW3D30) and 1 arc-second Shuttle Radar Topography Mission (SRTM) C-band, recently released optical stereoscopic and InSAR GDEMs by Japan Aerospace Exploration Agency (JAXA) and US National Aeronautics Space Administration (NASA), were comprehensively analyzed.

When using a DEM, the quality is the most significant fact which has a vital importance on the results. A low quality model may cause misleading interpretations and depending decision mechanism. Because of that, the assessment of

Editorial handling: M. Kasser

✉ Umut G. Sefercik
sefercik@beun.edu.tr

[1] Department of Geomatics Engineering, Faculty of Engineering, Zonguldak Bülent Ecevit University, Zonguldak, Turkey

[2] Department of Geomatics Engineering, Graduate School of Natural and Applied Sciences, Zonguldak Bülent Ecevit University, Zonguldak, Turkey

space-borne DEM qualities is very essential research topic for scientific community (Aguilar et al. 2010; Zhao et al. 2011; Hladik and Alber 2012; Hobi and Ginzler 2012). In the quality assessment of a DEM, many parameters should be considered. For instance, the absolute geolocation accuracy of space-borne DEMs cannot be as high as aerial DEMs or ground survey DEMs but they offer larger coverage depending upon the orbital height, low cost, and time-saving processing. That is why the comparison of DEMs which are provided by the similar acquisition technique (aerial or space-borne) is more sensible.

The primary objective of this paper is to demonstrate the country-scale discontinuities of commonly used AW3D30 and SRTM C-band GDEMs which are the most actual optical and SAR imagery. To show the coherence level of the GDEMs in different land cover classes and inclined terrain, Turkey was preferred as a convenient study area with its mountainous and multi-class topography. Turkey is located on four Universal Transverse Mercator (UTM) zones as 35–38, that is why mosaics of the GDEMs were produced by completing required transformations in these zones. In discontinuity analysis work flow, systematic horizontal offsets between GDEMs were estimated and eliminated by area-based cross correlation, absolute vertical standard deviations (σ_Z) and normalized median absolute deviations (NMAD) of height differences were calculated, frequency distribution of height differences between GDEMs was graphed, and height error maps which visualize the discontinuities were generated.

The paper was organized as follows: the topographic characteristics of the study area were given in the "Study area" section. Imaging geometries of ALOS and SRTM missions are presented in the "Imaging geometries of the satellites" section and analyzing methodology is described in the "Methodology" section. Results are given in the "Results" section followed by the conclusions.

Study area

Turkey is a transcontinental country in Eurasia represented with four UTM zones (35–38). The country has a rolling topography and the highest point is Ararat Mountain with 5137 m. The study area and its slope map are shown in Fig. 1a and b.

Imaging geometries of the satellites

SRTM was flown on board the space shuttle endeavor in February 2000 and its duration was 11 days in space. Endeavor (SRTM) was placed on a 233-km orbit height with an inclination of 57°. SRTM was a joint project between NASA, the National Imagery and Mapping Agency (NIMA), and the German Aerospace Center (DLR). The Italian Space Agency was cooperating with DLR. The aim of SRTM was to produce a homogenous, high-resolution GDEM for 80% of the Earth's land surface between 60° northern and 56° southern latitudes except pole zones. Based on the mission, height values with a spacing of 1 arc-second (~ 30 m) and 3 arc-second (~ 90 m) have been generated. During the mission, two different antennas were installed on board the shuttle. The main antenna length was 12 m and located in cargo bay and it acted as transmitter and receiver. The second one was an outboard antenna or slave antenna fixed at the end of 60 m long mast and was only a receiver. The 5.6-cm wavelength (λ) C-band had capability for ScanSAR mode where the antenna beam is electronically steered towards different elevation angles in a repeated stepwise fashion. Thus, four narrow but overlapping sub-swath were imaged quasi simultaneously to form a 225 km wide swath (Bamler 1999). With C-band 119.51 million km^2 were imaged corresponding to 99.97% of the target area. The C-band has nearly a complete coverage and 94.6% of the mapped area is covered at least twice and approximately 50% at least three times. Because of the radar layover distortion in very steep areas, gaps are available in 0.15% of the final DEM (Sefercik and Jacobsen 2006).

SRTM used the first space-borne single-pass InSAR which is the study of interference patterns accomplished by combining two sets of signals achieved in a single-pass. A suite of sensors is responsible for measuring and controlling the proper alignment of the secondary antenna with respect to the main antenna and the attitude and position of the interferometric system in orbit. A star tracker measured the orientation of the interferometric system in orbit, which was supported by an inertial reference unit consisting of three axis gyros. An optical tracker of the secondary antenna which is a video camera and LED targets allowed a relative 3-axis measurement of the boom antennas. Additionally, two GPS antennas, one on the main antenna structure the other one on the secondary, provided 0.8 m orbital position accuracy determination and furthermore, a time reference for the radar with an accuracy of 100 μs. The data acquisition by SRTM is based on the direction perpendicular to the orbit and the distance. The determination of the location based on distances is causing some radar distortions in inclined terrain. Layover mixes the radar signals and there is no possibility of a correct reconstruction in such steep parts. Shadows, due to higher incidence angle of SAR, cause areas with no information. The compression of the information by foreshortening is reducing the information in these parts.

ALOS was built by JAXA and launched on January 24, 2006 from Tanegashima Space Center, Japan. The satellite has three basic components for data acquisition. These are panchromatic remote sensing instrument for stereo mapping (PRISM), advanced visible and near infrared radiometer- type two (AVNIR-II), and phased array type L-band synthetic aperture radar (PALSAR). For the acquisition of stereoscopic

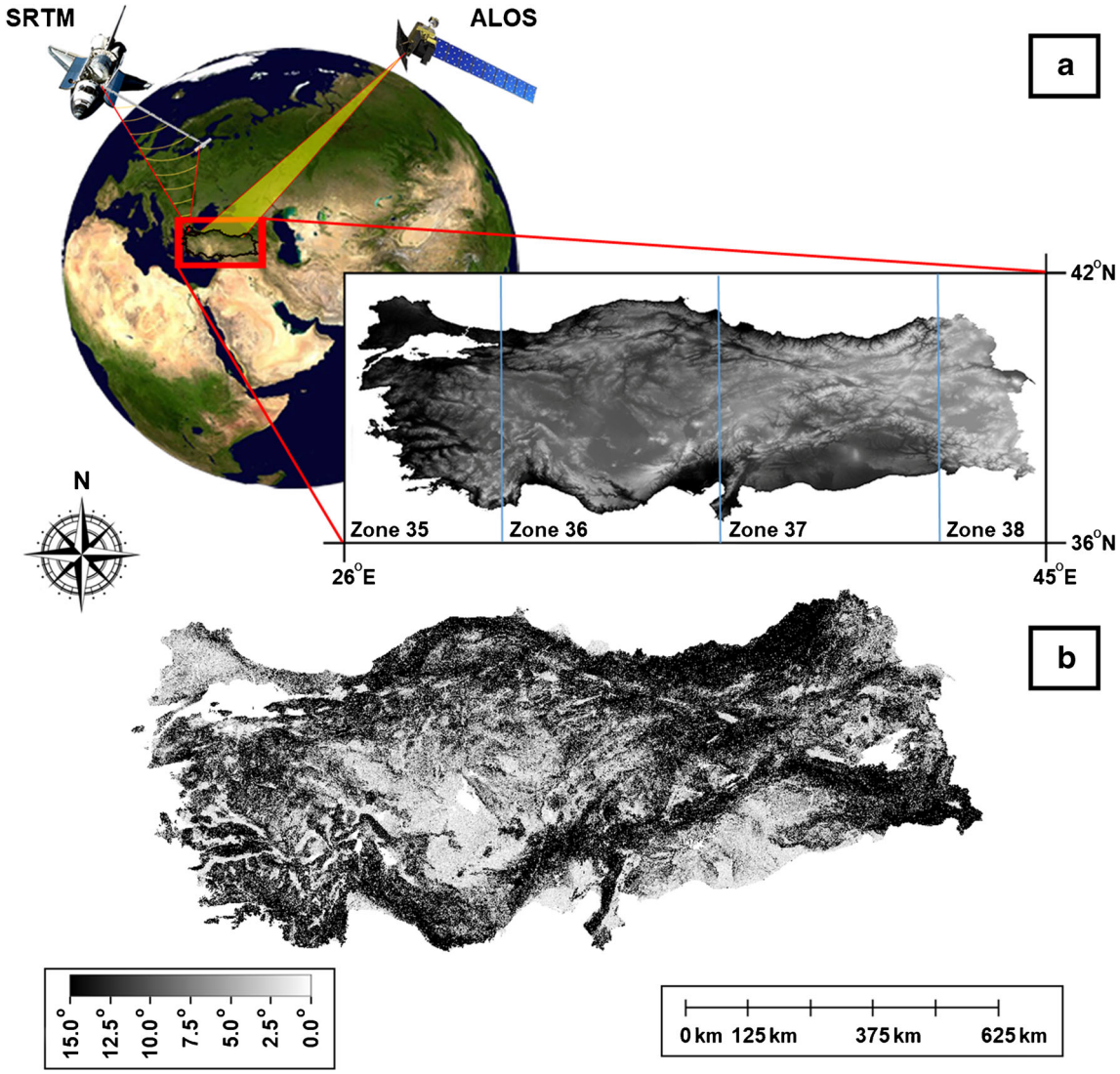

Fig. 1 The study area (**a**) and its slope map (**b**).

image, PRISM has three independent telescopes for nadir (70 km swath), forward, and backward (35 km swath per each) views. The triplet telescopes are used for push-broom scanning and each consists of three mirrors and several charged couple device (CCD) detectors. With 2.5 m ALOS prism images acquired between 2006 and 2011, AW3D30 GDEM was generated. With the advantage of 2.5 m spatial resolution stereo prism imagery, the topographic estimation performance of AW3D30 is higher than other similar grid DEMs such as Sentinel-1A and SRTM C-band (Sefercik et al. 2018). As other optical DEMs, AW3D30 has also problems of the gray value distribution in the forest areas (Buyuksalih and Jacobsen 2005). In the forest, due to low correlations, the problems are occurred in image matching. Inclined topography and shadow areas also cause misidentifications. Figure 2 presents the imaging geometries of SRTM and ALOS Prism missions.

As mentioned, SRTM uses two antennas at different locations to measure the difference in range to the surface in single pass. The phase difference between two different antennas can be calculated by Eq. 1 or 2:

$$\Delta\phi = -(\alpha 2\pi/\lambda)(r_1 - r_2) \quad (1)$$

$$\Delta\phi = -(\alpha 2\pi/\lambda)(\mathrm{B}\sin(\theta - \alpha)) \quad (2)$$

In Eq. 1, λ is the radar wavelength (5.6 cm for C-band), r_1 and r_2 are the radar ranges between antennas and the observing object, $\alpha = 2$ for standard repeat-track interferometry and $\alpha = 1$ when the signal is transmitted out of one antenna and simultaneously received through two different antennas separated in elevation, such as in the case of SRTM. In Eq. 2, B is the baseline separating the antennas and θ is the radar look angle. The specifications of the missions and GDEMs are presented in Table 1.

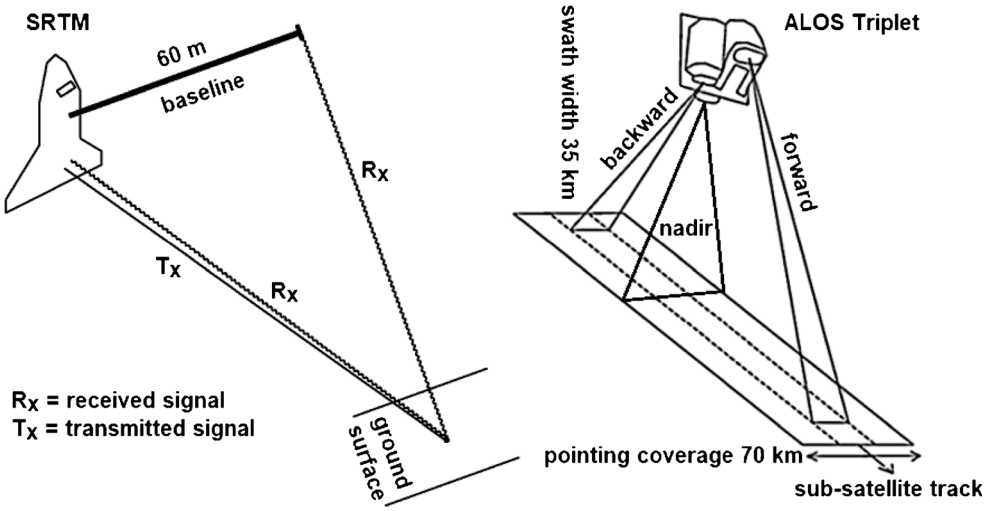

Fig. 2 SRTM and ALOS Prism imaging geometries

Methodology

The applied methodology is given in the following work flow (Fig. 3). Due to country-scale analysis, 48 tiles were determined considering the huge amount of data. The tiles were analyzed separately and the results were combined. The area was classified into four groups regarding the land cover and terrain slope (Fig. 4). The groups were open areas, forest, water, and inclined areas. The horizontal and vertical coherency analyses were realized separately for each group. The study area was classified by raster-vector transformation of raster Turkey maps obtained from governmental offices and the geolocation accuracies of these maps are under one pixel which is sufficient for our analysis. In addition, we tested the geolocation accuracies of the maps by matching coastal lines.

For analyzing the discontinuities of AW3D30 and SRTM, some pre-processing steps need to be applied. First, the vertical datum has to be fixed as either the geoid or ellipsoid, and geoid undulations have to be calculated if required. Second, the coordinate systems of the DEMs must be the same and the horizontal offsets which occur due to horizontal geolocation errors of both models must be compensated. The main rule of a correct vertical accuracy assessment is 100% horizontal overlap of compared DEMs. A horizontal shift influences the height by Eq. 3. In the equation, DZ is the vertical error, DL is the horizontal shift, and α is the terrain slope.

$$DZ = DL \times \tan(\alpha) \tag{3}$$

In the study, the common coordinate system and the datum were Universal Transverse Mercator (UTM) and World Geodetic System 1984 (WGS84), and the geoid undulations were calculated based on orthometric heights. The horizontal geolocation errors were determined by area-based matching using cross-correlation (Baltsavias et al. 2008; Alobeid et al. 2010) and eliminated by horizontal shifting. Table 2 shows the estimated and eliminated horizontal geolocation errors in X and Y directions in each zone separately. In the analysis, SRTM was used as the master (reference) DEM and AW3D30 was preferred as slave. This choice is not significant

Table 1 Specifications of the missions and GDEMs

Specification	Mission	
	SRTM	ALOS
Made in	USA/Germany	Japan
Launch date	11.02.2000	24.01.2006
Sensor/band	C-band	Prism
Spatial resolution of images	20 m × 30 m (Az × Rg)	2.5 m
GDEM resolution	1 arc-second (~ 27 m)	1 arc-second (~ 27 m)
Coverage	Global (except pole zones)	Global (except pole zones)
Datum	UTM WGS84	UTM WGS84
Raw data acquisition date	2000	2006–2011
Version and version date	V4/2015	1.1/2017

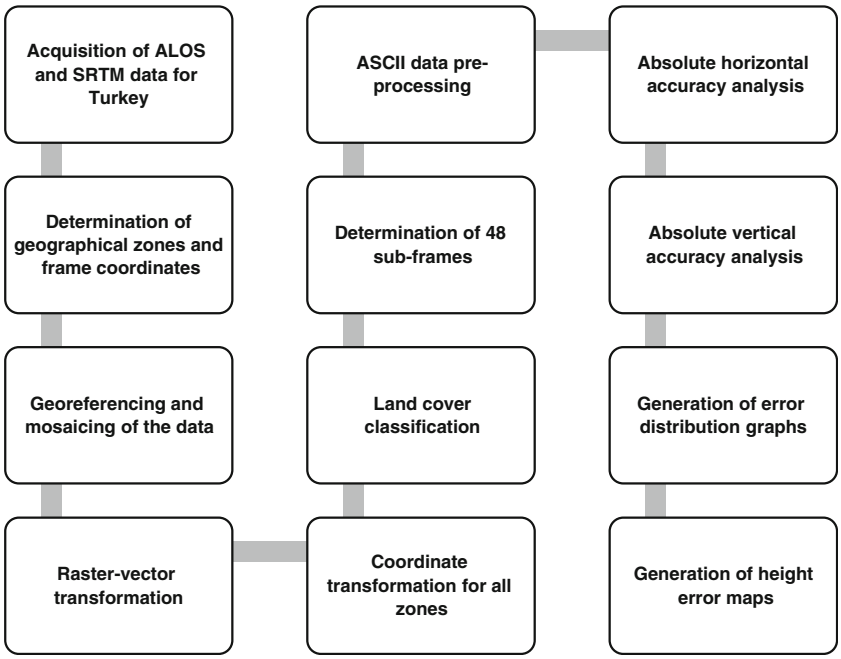

Fig. 3 Methodology of the study

and only changes the direction of the errors and not the magnitude. As can be seen in Table 2, horizontal errors are around one pixel (30 m) in Y and one third of a pixel in X direction.

In model-to-model DEM vertical accuracy analysis, root mean square error (RMSE) and the standard deviation of height discrepancies (RMSZ or σ_Z) are used (Eqs. 4–7). In the equations, n is the number of pixels (comparison points). In this study, σ_Z that estimates the vertical accuracy with a 68% probability level was used as the main evaluation criteria.

$$RMSZ = \sqrt{\frac{\sum_{i=1}^{n} \Delta Z_i^2}{n}} \tag{4}$$

If the arithmetic mean of the height discrepancies is given as

$$\mu = \frac{\sum_{i=1}^{n} \Delta Z_i}{n} \tag{5}$$

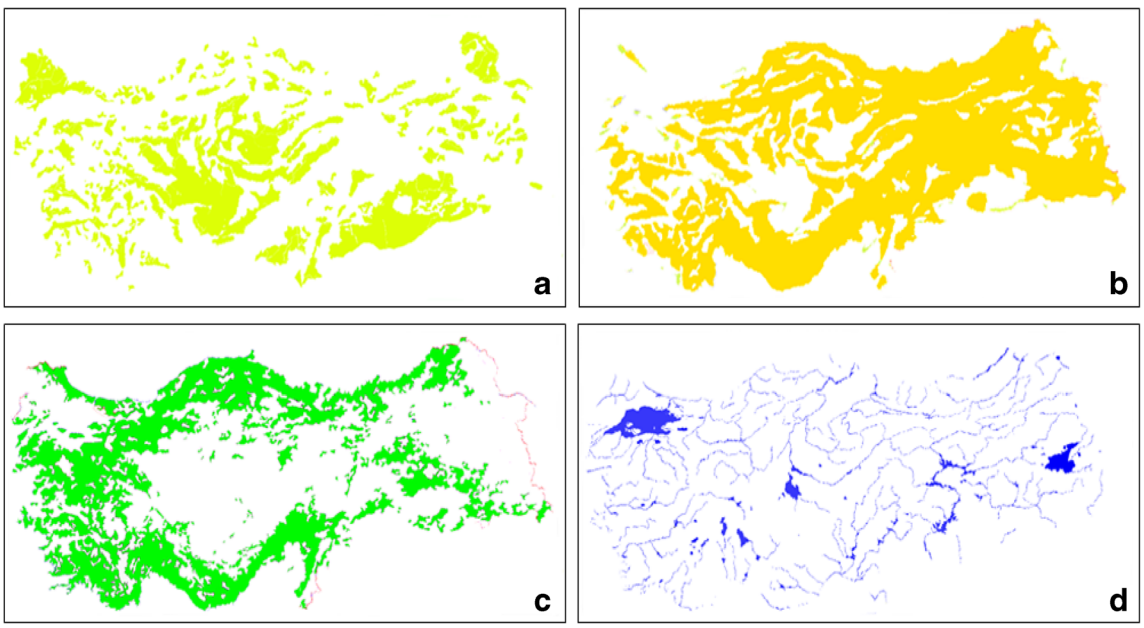

Fig. 4 Land cover classes and inclined terrain: **a** open and uninclined, **b** inclined areas, **c** forest, **d** water

Table 2 Estimated and eliminated horizontal geolocation errors (μ is the average)

Master DEM	Slave DEM	Zone (°)	ΔX (m)	ΔY (m)
SRTM (30 m)	AW3D30 (30 m)	35	30.44	− 31.34
		36	10.30	− 31.58
		37	3.64	− 32.53
		38	2.75	− 30.42
		μ	11.78	− 31.47

The σ_Z of the height differences between SRTM and AW3D30 is equal to

$$\sigma_Z{}^2 = RMSZ^2 - \mu^2 \tag{6}$$

Or,

$$\sigma_Z = \sqrt{\frac{\sum_{i=1}^{n} (\Delta Z_i - \mu)^2}{n-1}} \tag{7}$$

In addition to σ_Z, the normalized median absolute deviation (NMAD) of the height discrepancies was used as the second absolute vertical accuracy metric. NMAD is the derivative of median absolute deviation (MAD), which is a robust measure of the variability of a univariate sample of quantitative data. MAD and NMAD are calculated by Eqs. 8 and 9, where $\widetilde{X_j}$ is the median of the univariate data set of height discrepancies ($\Delta Z_1, \Delta Z_2, \ldots, \Delta Z_n$) and $\widetilde{X_i}$ is the median of height discrepancies from $\widetilde{X_j}$.

$$MAD = \widetilde{X_i}\left[\left|\Delta Z_i - \widetilde{X_j}(\Delta Z_j)\right|\right] \tag{8}$$

$$NMAD = 1.4826 \times (MAD) \tag{9}$$

In the case of normally distributed height discrepancies between compared DEMs, NMAD is identical to σ_Z and have 68% probability level. In abnormal distribution, the NMAD is bigger than σ_Z, although a robust estimator, NMAD, is not as sensitive in regard to σ_Z for the determination of minor outliers in a large data set (Hellerstein 2008).

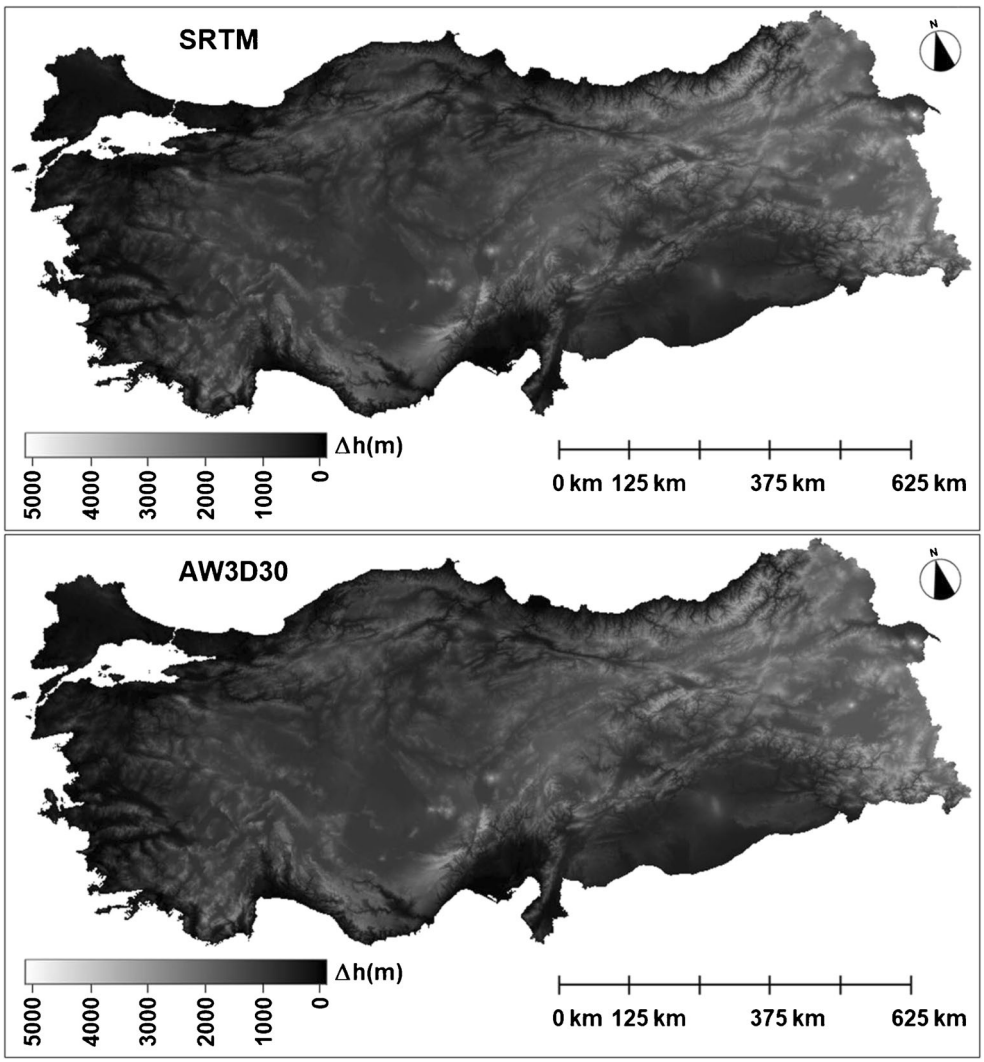

Fig. 5 Mosaicked SRTM and AW3D30 DEMs

Table 3 Estimated absolute vertical geolocation errors in land cover classes

Master DEM	Slave DEM	Land cover class	σ_Z (m)	NMAD (m)
SRTM (30 m)	AW3D30 (30 m)	Open	3.55	2.50
		Forest	4.62	3.18
		Water	4.07	2.50
		Inclined	4.39	3.06

As for visual validations, color-coded height error maps of SRTM and AW3D30 were generated by calculating the differential models with Eq. 10. The height error scales were prepared for ± 12 m which was detected as the maximum height difference between SRTM and AW3D30 after the elimination of systematic bias.

$$Height\ Error\ Map = DEM_{SRTM} - DEM_{AW3D30} \quad (10)$$

Results

One arc-second mosaicked SRTM and AW3D30 Turkey GDEMs are illustrated in Fig. 5. As expected, depending up on the country scale, the GDEMs look similar which demonstrates that the topographic representation capabilities of analyzed GDEMs are not considerably different. However, in country scale, it is impossible to recognize the height differences under hundred meters in visual way that's why numerical results will be more helpful to interpret the coherency between two GDEMs. Tables 3, 4, 5, and 6 present the estimated absolute vertical geolocation errors between two GDEMs. In the tables, the influence of land cover and terrain inclination on the coherence are clearly seen.

The effect of land cover classes on the vertical accuracy is defined by three different accuracy types as fundamental vertical accuracy, supplemental vertical accuracy, and consolidated vertical accuracy. Fundamental vertical accuracy is calculated based on the results in open areas which represent the bare topography. In normal case, it is the most reliable way to understand the accuracy level of a DEM in first impression due to comparing 100% same topography with a reference model without non-terrain objects such as buildings and forest. On the other hand, fundamental vertical accuracy is an insufficient indicator to assess the performance of a DEM derived by remotely sensed data. For a space-borne raster DEM, main challenges are caused by built-up areas with suddenly changed elevations and narrow streets and forest covered areas. For GDEMs, the problems in built-up areas are not as significant as in forest due to large grid intervals as in SRTM and AW3D30. In 30-m grid, single buildings and narrow streets cannot be represented and determined as smoother that is why sudden elevation changes are automatically eliminated.

Supplemental vertical accuracy represents the vertical accuracy of a DEM calculating average mean of vertical accuracies of land cover classes of the study area except open areas. Supplemental vertical accuracy helps to validate the 3D non-terrain object description potential of a space-borne DEM. Finally, consolidated vertical accuracy is the arithmetic mean of all specified land cover classes in the study area (Sefercik et al. 2015).

As shown in Table 3, in the open areas, the coherency is in the highest level and around 3.5 m as σ_Z and 2.5 m as NMAD and these values also correspond to fundamental vertical accuracy in Table 4. In the other land cover classes, the coherence decreases between 4 and 4.5 m as σ_Z and 3 and 3.5 m as NMAD which correspond to supplemental vertical accuracy in Table 4. Comparing fundamental vertical accuracy and supplemental vertical accuracy, it is clear that SRTM and AW3D30 GDEMs have difficulties to describe the non-open topographies. Nevertheless, the height differences are under 5 m which indicates a well coherence between GDEMs.

As mentioned before, in Turkey, a mountainous topography is dominant and the orthometric elevation reaches up to 5137 m. In Table 5, the considerable influence of terrain inclination is presented by calculating the coherence in nearly flat areas (slope $\leq \sim 6°$). In uninclined topographies, the coherency arises to 2.6 m as σ_Z and 2.1 m as NMAD in open areas correspond fundamental vertical accuracy in Table 6. In the uninclined areas in other land cover classes, the coherence is between 3 and 4 m as σ_Z and 2.5 and 3 m which correspond to supplemental vertical accuracy in Table 6. When, the results of inclined and uninclined areas are compared (please check

Table 4 Estimated absolute vertical geolocation errors as vertical accuracy, supplemental vertical accuracy, and consolidated vertical accuracy

Master DEM	Slave DEM	Coherence indicator	σ_Z (m)	NMAD (m)
SRTM (30 m)	AW3D30 (30 m)	Fundamental vertical accuracy	3.55	2.50
		Supplemental vertical accuracy	4.36	2.91
		Consolidated vertical accuracy	4.16	2.81

Table 5 Effect of terrain inclination in land cover classes

Master DEM	Slave DEM	Land cover class	σ_Z (m) slope < $\tan^{-1}$ 0.1	NMAD (m) slope < $\tan^{-1}$ 0.1
SRTM (30 m)	AW3D30 (30 m)	Open	2.60	2.13
		Forest	4.14	3.10
		Water	3.47	2.66

Table 6 Effect of terrain inclination as fundamental vertical accuracy, supplemental vertical accuracy, and consolidated vertical accuracy

Master DEM	Slave DEM	Land cover class	σ_Z (m) slope < $\tan^{-1}$ 0.1	NMAD (m) slope < $\tan^{-1}$ 0.1
SRTM (30 m)	AW3D30 (30 m)	Fundamental vertical accuracy	2.60	2.13
		Supplemental vertical accuracy	3.80	2.88
		Consolidated vertical accuracy	3.40	2.63

Table 3 for inclined areas and consolidated vertical accuracy in Table 6), the influence of terrain inclination is ~ 1 m as σ_Z and ~ 0.5 m as NMAD which means terrain slope has more influence on NMAD.

The frequency distribution of height differences between SRTM and AW3D30 GDEMs is an important indicator for homogenous coherency. In Figs. 6 and 7, the distribution between SRTM and AW3D30 is shown for land cover classes

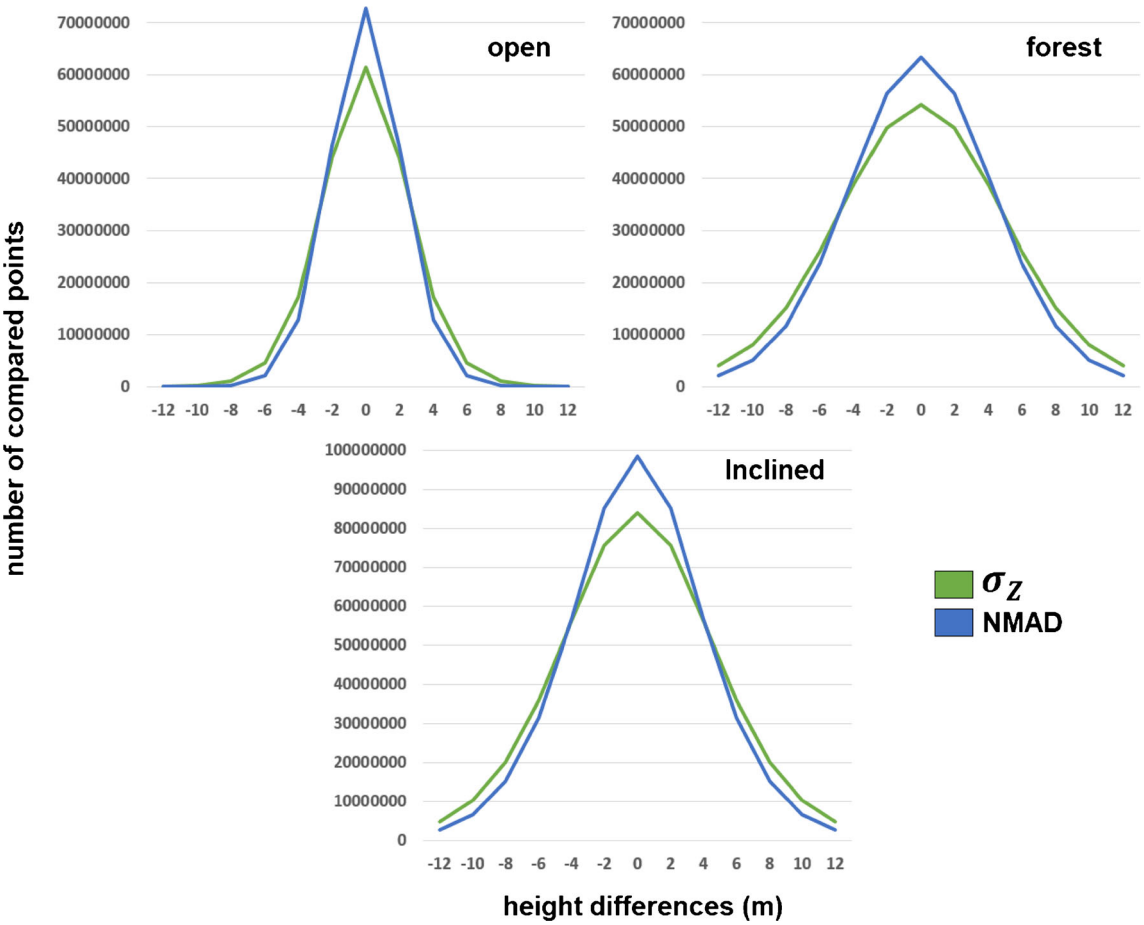

Fig. 6 Frequency distribution of height differences based on σ_Z and NMAD

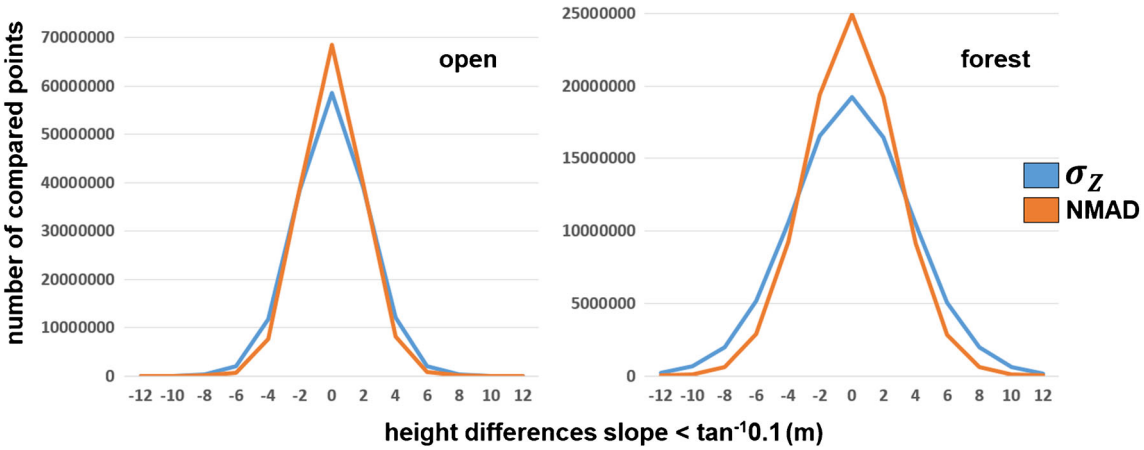

Fig. 7 Frequency distribution of height differences based on σ_Z and NMAD in uninclined parts (slope < $\tan^{-1}0.1$)

and inclined regions respectively. In case of normally distributed height discrepancies, NMAD is identical to σ_Z, in fact in reality and not under the same accuracy conditions, such as those caused by different terrain inclinations and larger discrepancies, in most cases, NMAD is smaller than σ_Z. As a consequence, NMAD is continuously smaller than σ_Z both in Figs. 6 and 7 which indicates a normal distribution. In Figs. 6 and 7, the peaks of height differences are around zero which means full coherence. In addition, the distributions are symmetric which is also another indicator of a normal distribution. Another significant point is ± 12 m limit of height differences which means the level of outliers. As stated in other words, all of the pixels in raster SRTM and AW3D30 GDEMs have ≤ 12 m height difference which demonstrates a good coherence.

Figure 8 shows the height error map of SRTM and AW3D30 GDEM on Turkey. In the height error map, the location of coherent and incoherent parts is clearly presented by ± 12 m color scale. The coherence is high in light and low in dark parts. Generated height error map exhibits the problems of GDEMs in inclined and forest regions. Almost all of dark parts are located in the mountains and the dense forests of Turkey. To determine the effect of land cover and terrain inclination, the classified height error maps are presented in Fig. 9.

If the height error map is examined in detail, the inverse coherence in sequential vertical lines can be noticed. In contrast to optical imaging, SAR acquires space-borne data using ascending (south to north) and descending (north to south) passes in near-polar orbits. In ascending and descending passes, amount of acquired data is different depending on sun-light and darkness. In darkness, the solar panels cannot generate power that is why more data is acquired in sunlight. The height error map demonstrates the effect of ascending and descending orbits on the topographic description potential of SAR data clearly. Line by line,

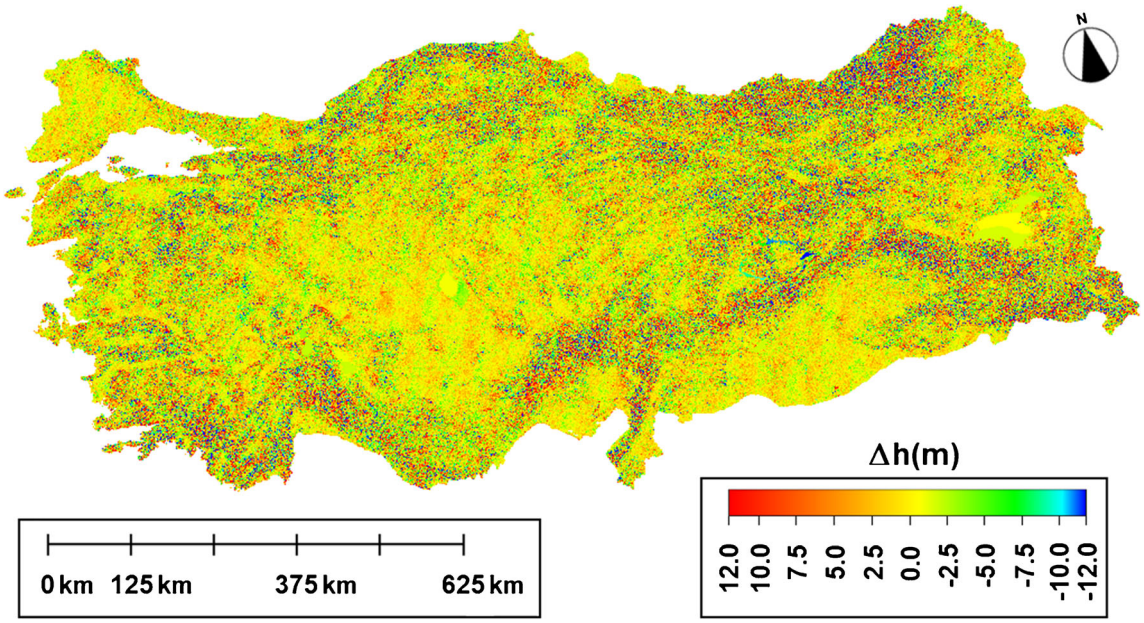

Fig. 8 Height error maps of SRTM and AW3D30 GDEMs

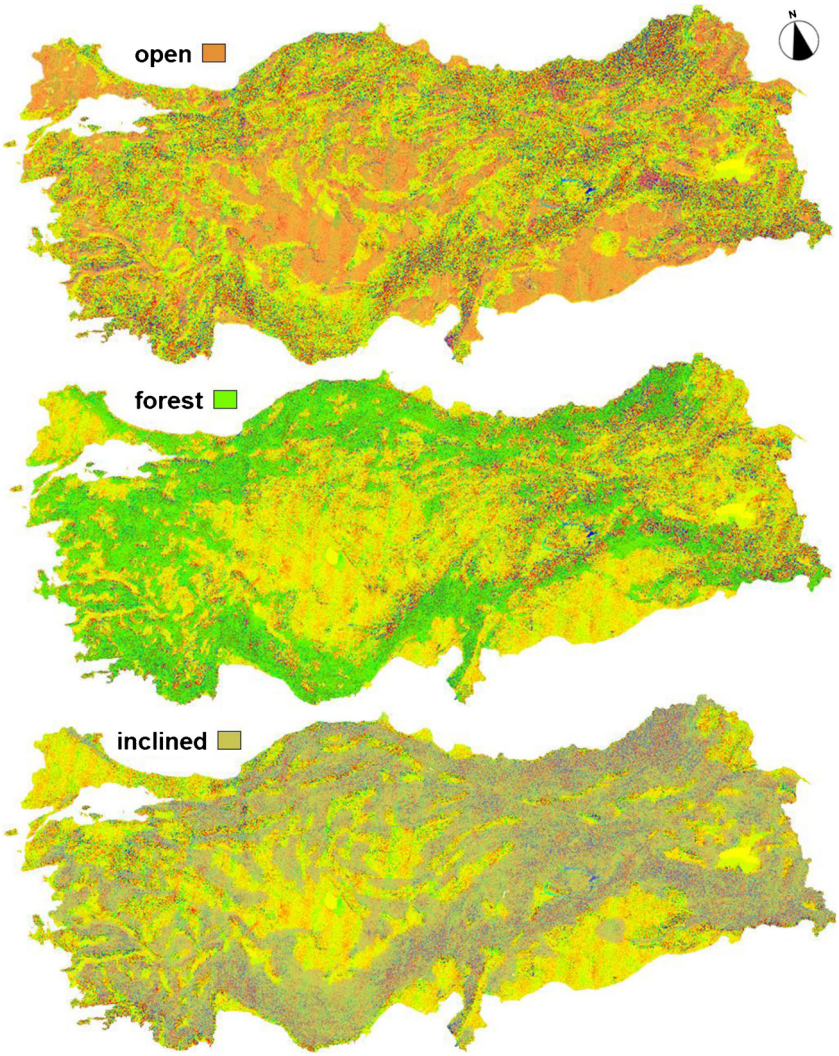

Fig. 9 Classified height error maps of SRTM and AW3D30 GDEMs

the height differences between SRTM and AW3D30 GDEMs reverse as red tones and green tones.

In classified height error maps, the influence of forest and inclined topographies is clear. Particularly, inclined areas are the main cause of low coherency. Although the grid spacing of AW3D30 GDEM is approx. 30 m, it was generated from ALOS Prism imagery with 2.5 m ground sampling distance (GSD) that is why the description of the topography is more detailed than SRTM GDEM, derived from 30 m × 20 m (azimuth × range) GSD C-band SAR imagery (Sefercik et al. 2018). This situation is the main cause of low coherency in inclined and forest regions.

Conclusions

SRTM and AW3D30 are two of the most demanded GDEMs in land-related applications. In this study, discontinuities between equal gridded SRTM and AW3D30 GDEMs were comprehensively investigated by means of visual and quantitative analysis in country scale. Regarding the challenges of space-borne remote sensing imaging geometries, the study area which has a mountainous topography and dense forest coverage was preferred. In this manner, coherence between GDEMs in hard conditions was determined. In horizontal geolocation analysis, offsets between GDEMs were estimated by areal based cross correlation and eliminated by horizontal shifting. After 100% horizontal overlapping, vertical coherence level between GDEMs was calculated by means of standard deviation and normalized median absolute deviation of pixel height differences. The results demonstrated that the coherence of SRTM and AW3D30 is ≤ 1 pixel (30 m) in horizontal direction and ± 12 m in height. The influence of land cover and terrain inclination was visualized by error distribution graphics and height error maps. In the frequency distribution of height differences graphics, a normal and symmetric distribution was specified. Effect of ascending and descending flying orbits (aspects) on SAR imaging was clearly demonstrated.

Overall, in open and uninclined areas, the coherence of SRTM and AW3D30 GDEMs is high and any of them can be utilized in the applications. However, in forest and inclined regions, scientific and commercial users should be very careful in

preferring the correct GDEM. Although freely achieved in equal grid spacing, the topographic description potentials of GDEMs are different due to 2.5 m GSD ALOS Prism and 30 m × 20 m C-band images. Larger GSD causes smoothing effect on SRTM GDEM that is why AW3D30 will be more useful in the applications conducted in forest and inclined topographies.

Acknowledgements We would like to thank NASA and JAXA for freely supporting 1 arc-second SRTM C-band and AW3D30 GDEMs.

3.References

Aguilar FJ, Mills JP, Delgado J, Aguilar MA, Negreiros JG, Perez JL (2010) Modelling vertical error in Lidar-derived digital elevation models. ISPRS J Photogramm Remote Sens 65(1):103–110

Alobeid A, Jacobsen K, Heipke C (2010) Comparison of matching algorithms for DSM generation in urban areas from IKONOS imagery. Photogramm Eng Remote Sens 76(9):1041–1050

Bahuguna IM, Kulkarni AV (2005) Application of digital elevation model and orthoimages derived from IRS-1C Pan stereo data in monitoring variations in glacial dimensions. J Indian Soc Remote Sens 33(1): 107–112

Baltsavias E, Gruen A, Eisenbeiss H, Zhang L, Waser T (2008) High-quality image matching and automated generation of 3D tree models. Int J Remote Sens 29(5):1243–1259

Bamler R (1999) The SRTM mission: a worldwide 30m resolution DEM from SAR interferometry in 11 days. Photogrammetric Week 99: 145–154

Bullard JE, White K, Livingstone I (2011) Morphometric analysis of aeolian bedforms in the Namib Sand Sea using ASTER data. Earth Surf Process Landf 36(11):1534–1549

Buyuksalih G, Jacobsen K (2005) DEM generation and validation based on optical satellite systems. EARSeL Workshop on 3D-Remote Sensing, Porto, Portugal, p 7 (on CD-ROM)

Carvalho O, Guimaraes R, Freitas L (2010) Urbanization impacts upon catchment hydrology and gully development using mutli-temporal digital elevation data analysis. Earth Surf Process Landf 35(5):611–617

Cuartero A, Felicisimo AM, Ariza FJ (2005) Accuracy, reliability, and depuration of SPOT HRV and Terra ASTER digital elevation models. IEEE Trans Geosci Remote Sens 43(2):404–407

DeLong SB, Prentice CS, Hilley GE, Ebert Y (2012) Multitemporal ALSM change detection, sediment delivery, and process mapping at an active earthflow. Earth Surf Process Landf 37(3):262–272

Gianinetto M (2009) Influence of the elevation accuracy in the updating of large scale geo-databases in mountain urban areas using IKONOS images. J Appl Remote Sens 3:033536

Heckmann T, Bimbose M, Krautblatter M, Haus F, Becht M, Morshe D (2012) From geotechnical analysis to quantification and modelling using Li-DAR data: a study on rockfall in the Reintal catchment, Bavarian Alps, Germany. Earth Surf Process Landf 37(1):119–133

Hellerstein J M (2008). Quantitative data cleaning for large databases. Technical Report Presented at United Nations Economic Commission for Europe (UNECE), p. 42

Hladik C, Alber M (2012) Accuracy assessment and correction of a LIDAR-derived salt marsh digital elevation model. Remote Sens Environ 121:224–235

Hobi ML, Ginzler C (2012) Accuracy assessment of digital surface models based on WorldView-2 and ADS80 stereo remote sensing data. Sensors 12(5):6347–6368

Kaczynski R, Majde A, Ewiak I (2004) Accuracy of DTM and Ortho generated from IKONOS Stereo images. In Proceeding of the ISPRS XX congress, Instanbul, Turkey 463–464

Lee HY, Kim T, Park W, Heung KL (2003) Extraction of digital elevation models from satellite stereo images through stereo matching based on epipolarity and scene geometry. Image Vis Comput 21(9):789–796

Li R, Zhou G, Schmidt NJ, Fowler C, Tuell G (2002) Photogrammetric processing of high-resolution airborne and satellite linear array stereo images for mapping applications. Int J Remote Sens 23(20): 4451–4473

Martino C, Nico G, Schiattarella M (2009) Quantitative analysis of InSAR digital elevation models for identification of areas with different tectonic activities in southern Italy. Earth Surf Process Landf 34(1):3–15

Radhadevi PV, Solanki SS, Nagasubramanian V, Mahapatra A, Sudheer RD, Jyothi MV, Krishna S, Saibaba J, Geeta V (2010) New era of Cartosat satellites for large scale mapping. Photogramm Eng Remote Sens 76(9):1031–1039

Schneider A, Gerke HH, Maurer T, Seifert S, Nenov R, Hüttl RF (2012) Evaluation of remotely-sensed DEMs and modification based on plausibility rules and initial sediment budgets of an artificially-created catchment. Earth Surf Process Landf 37(7):708–725

Sefercik UG, Jacobsen K (2006) Analysis of SRTM height models, 5. International Symposium Turkish-German Geodetic Days. Technical University, Berlin, Germany, p 6 (On CD-ROM)

Sefercik UG, Soergel U (2010) Comparison of high resolution InSAR and optical DEMs. EARSeL Joint SIG Workshop, Ghent (on CDROM)

Sefercik UG, Glennie C, Singhania A, Hauser D (2015) Area-based quality control of airborne laser scanning 3D models for different land classes using terrestrial laser scanning: sample survey in Houston, USA. Int J Remote Sens 36(23):5916–5934

Sefercik UG, Buyuksalih G, Atalay C, Jacobsen K (2018) Validation of Sentinel-1A And AW3D30 DSMs for the Metropolitan Area of Istanbul, Turkey. Journal of Photogrammetry, Remote Sensing and Geoinformation Science 86(3-4):141–155

Soergel U, Thoennessen U, Stilla U (2003). Visibility analysis of man-made objects in SAR image. In Proceeding of the 2nd GRSS/ISPRS joint workshop data fusion and remote sensing over urban areas, pp. 120–124

Soergel U, Michaelsen E, Thiele A, Cadario E, Thoennessen U (2009) Stereo analysis of high-resolution SAR ımages for building height estimation in case of orthogonal aspect directions. ISPRS J Photogramm Remote Sens 64(5):490–500

Toutin T (2002) DEM from stereo Landsat 7 ETM+ data over high relief areas. Int J Remote Sens 23(10):2133–2139

Toutin T (2008) ASTER DEMs for geomatic and geoscientific applications: a review. Int J Remote Sens 29(7):1855–1875

Zhao SM, Cheng WM, Zhou CH, Chen X, Zhang S, Zhou Z, Liu H, Chai H (2011) Accuracy assessment of the ASTER GDEM and SRTM3 DEM: an example in the Loess Plateau and North China Plain of China. Int J Remote Sens 32(23):8081–8093